Mass yield curves in low-energy proton-induced fission of ^{233}U, ^{235}U, ^{236}U, ^{237}Np, ^{239}Pu, ^{242}Pu, ^{244}Pu, ^{241}Am, and ^{243}Am

T. Ohtsuki,[1,2],* Y. Nagame,[2] K. Tsukada,[1] N. Shinohara,[2] S. Baba,[2] K. Hashimoto,[2] I. Nishinaka,[1] K. Sueki,[1] Y. Hatsukawa,[2] K. Hata,[2] T. Sekine,[2] I. Kanno,[2] H. Ikezoe,[2] and H. Nakahara[1]

[1]*Department of Chemistry, Faculty of Science, Tokyo Metropolitan University, Minami-Ohsawa, Hachioji, Tokyo 192-03, Japan*

[2]*Japan Atomic Energy Research Institute (JAERI), Tokai, Ibaraki 319-11, Japan*

(Received 25 April 1991)

Mass yield curves in low-energy proton-induced fission of ^{233}U, ^{235}U, ^{236}U, ^{237}Np, ^{239}Pu, ^{242}Pu, ^{244}Pu, ^{241}Am, and ^{243}Am were investigated in the energy range of 8–32 MeV. The gross features of mass yield curves were compared either at the same excitation energy or for the same charge of the compound nucleus with different neutron number. The results are briefly discussed in terms of (1) the weighted mean mass number of the light and heavy asymmetric peak, (2) the FWHM of the heavier asymmetric peak, and (3) the peak-to-valley ratio.

I. INTRODUCTION

From early days in the fission study, mass yield curves of fission products have been extensively studied by both experimentalists and theorists. But even now, more than half a century since its discovery, their fundamental understanding is still meager. General features of mass yield curves observed in low-energy fission of actinides are summarized in several reviews [1–4]. Some characteristics of the fission with $90 \leq Z < 100$ are (1) they are double humped, indicating the preference of predominantly asymmetric mass division, (2) symmetric mass division becomes more favored with increasing incident energy, and (3) the mean mass number of the heavy fission products always falls in between $A = 134$ and 142. More recent experiments on spontaneous fission of very heavy actinides with $Z = 100-104$ have indicated that the preference of asymmetric or symmetric mass division is critically dependent on the atomic number and/or the neutron number of the fissioning nucleus [5].

In the present work, the effect of Z and N of the fissioning nucleus on the mass yield curve has been investigated for proton-induced fission of light actinides by varying the incident proton energy. The aim is to study more extensively the systematic variation of mass yield curves as a function of the (Z,N) of the fissioning nucleus and the excitation energy in order to elucidate how strongly some basic physical quantities affect the mass division in fission. Detailed studies on the variation of mass yield curves as a function of the mass number for the same fissioning isotope have reported only for a few

TABLE I. Reactions of proton-induced fissions and the range of the incident energy.

Reaction	E_{proton} (MeV)
^{232}Th+p[a]	9–22
^{233}U+p	8–16
^{235}U+p	9–18
^{236}U+p	9–16
^{238}U+p[b]	10–25
^{237}Np+p	10–32
^{239}Pu+p	10–16
^{242}Pu+p	12,18
^{244}Pu+p	10–18
^{241}Am+p	9–16
^{243}Am+p	10–16

[a]Kudo *et al.* from Ref. [17].
[b]Hamajima *et al.* from Ref. [18].

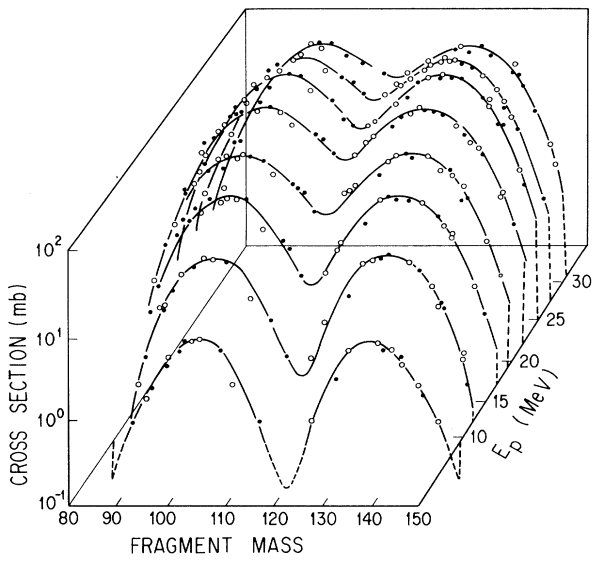

FIG. 1. Incident energy dependence of mass yield curve measured in proton-induced fission of ^{237}Np.

cases: 14.5-MeV neutron-induced fission of uranium isotopes (^{233,234,235,236,238}U) [6] and spontaneous fission of plutonium isotopes (^{236,238,240,242,244}Pu) [7]. Besides, as the experimental data on proton-induced fission are scarce, the results of the present work may be valuable for future nuclear technology.

In this paper, experimental data for targets of ^{233}U, ^{235}U, ^{236}U, ^{237}Np, ^{239}Pu, ^{242}Pu, ^{244}Pu, ^{241}Am, and ^{243}Am are presented and some gross features of mass yield curves are pointed out. More detailed analysis and discussion of the data will be given in a separate paper due to the limitation of space.

TABLE II. Nuclear properties of fission products.

Nuclide	Gamma-ray energy (keV)	Absolute γ intensity (γ/decay)	Half-life
^{85}Kr^{m}	151.2	0.746	4.48 h
^{87}Kr	402.6	0.494	76 min
^{88}Kr	196.3	0.263	2.48 h
^{91}Sr	1024.5	0.334	9.48 h
^{92}Sr	1384	0.900	2.7 h
^{93}Y	266.9	0.07	10.1 h
^{95}Zr	757	0.564	65 d
^{97}Nb[a]	658	0.985	16.9 h (^{97}Zr)
^{99}Tc^{m} [a]	140.5	0.907	66 h (^{99}Mo)
^{103}Ru	497.1	0.895	39.25 d
^{105}Rh	319	0.192	35.9 h
^{111}Ag	342	0.067	7.45 d
^{112}Ag[a]	617	0.429	21 h (^{112}Pd)
^{113}Ag	298.6	0.10	5.37 h
^{115}In^{m} [a]	336.3	0.497	53.5 h (^{115}Cd)
^{117}Cd^{g}	1303	0.184	2.49 h
^{117}Cd^{m}	1998	0.267	3.4 h
^{126}Sb	695	1.00	12.4 d
^{127}Sb	473	0.251	3.85 d
^{128}Sb	754	1.00	9.1 h
^{129}Sb	812.8	0.435	4.32 h
^{130}I	418	0.345	12.36 h
^{131}I	364.5	0.812	8.02 d
^{132}Te	228.2	0.88	78 h
^{132}I[a]	772.6	0.764	2.3 h
^{133}I	529.9	0.873	20.8 h
^{135}I	1260.4	0.303	6.59 h
^{135}Xe[a]	249.8	1.00	9.01 h
^{136}Cs	1048	0.80	13.0 d
^{139}Ba	165.9	0.188	83.2 min
^{140}Ba	537	0.244	12.8 d
^{140}La[a]	1596	0.965	40.2 h
^{141}La	1354	0.026	3.90 h
^{141}Ce	145.5	0.484	32.5 d
^{142}La	641.2	0.49	92.5 min
^{143}Ce	293.3	0.413	33 h
^{149}Nd	211.3	0.273	1.73 h
^{151}Pm	340.1	0.24	28.4 h
^{153}Sm	103	0.28	47 h

[a]To determine yield of the parent.

II. EXPERIMENTAL PROCEDURE AND DATA TREATMENT

The isotopic composition of each target was, according to the assay by the supplier, as follows: ^{243}Am target—^{243}Am 99.61%, ^{241}Am 0.11%, ^{244}Cm 0.28%; ^{242}Pu target—^{242}Pu 99.85%; ^{244}Pu target—^{244}Pu 97.89%, ^{239}Pu 0.03%, ^{240}Pu 0.68%, ^{241}Pu 0.07%, ^{242}Pu 1.33%. Other targets were more than 99.0% enrichment. After

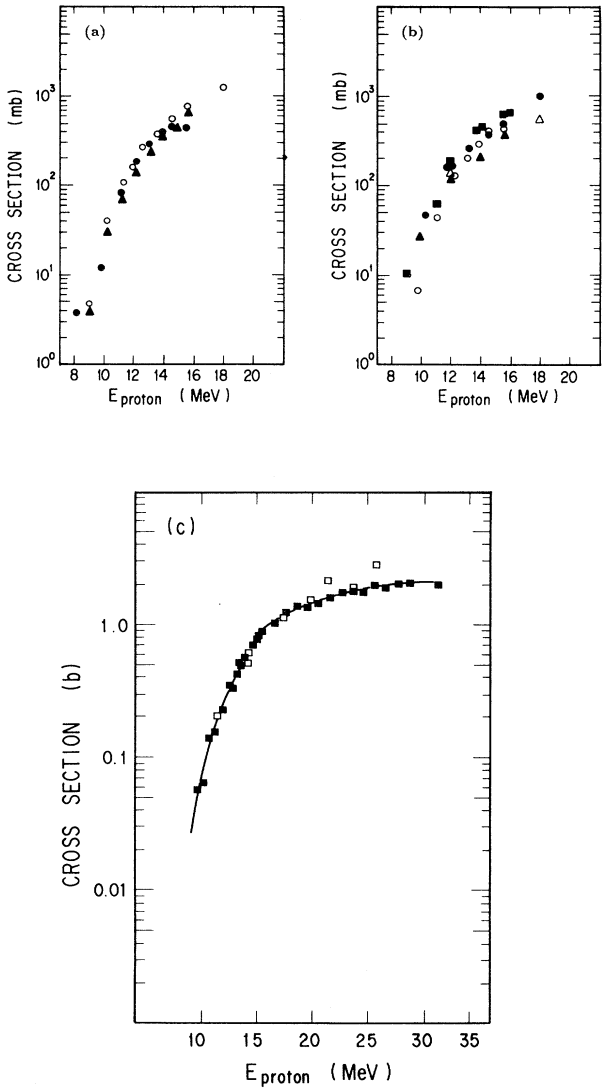

FIG. 2. (a) Fission cross section observed as a function of proton energy for U target; ● for ^{233}U, ○ for ^{235}U, and ▲ for ^{236}U. (b) Fission cross section observed as a function of proton energy for Pu and Am targets; ○ for ^{239}Pu, △ for ^{242}Pu, ● for ^{244}Pu, ■ for ^{241}Am, and ▲ for ^{243}Am. (c) Fission cross section observed as a function of proton energy for Np target; ^{237}Np. Solid squares are those obtained in this work, open squares are those reported by Polak and Aten (Ref. [16]).

TABLE III. Fission product yield of the proton-induced fission of ^{233}U.

Fission product	Incident proton energy 15.5 MeV (mb)	14.6 MeV (mb)	13.9 MeV (mb)	13.0 MeV (mb)	12.2 MeV (mb)	11.2 MeV (mb)	9.8 MeV (mb)	8.2 MeV (mb)
$^{85}Kr^{m}$	5.84±0.07	6.38±0.07	4.80±0.29	3.46±0.25	2.57±0.20	1.16±0.27	0.18±0.05	0.06±0.01
^{87}Kr	6.74±0.27	7.20±0.49	6.00±0.60	4.53±0.62	2.94±0.25	1.65±0.18	0.27±0.03	0.09±0.02
^{88}Kr	7.14±0.25	7.05±0.27	6.00±0.25	4.86±0.34	3.68±0.34	1.67±0.09	0.34±0.07	0.09±0.02
^{91}Sr	13.29±0.51	13.67±0.62	11.73±0.27	7.91±0.47	6.13±0.51	2.90±0.98	0.46±0.10	0.14±0.03
^{92}Sr	12.60±0.20	13.20±0.18	11.31±0.22	8.07±0.34	5.80±0.31	2.83±0.09	0.44±0.03	
^{93}Y		15.12±1.20	13.63±1.32	9.14±1.00	7.00±0.56	3.28±0.36	0.60±0.16	0.18±0.01
^{95}Zr	17.53±1.43	16.57±1.70	14.41±0.87	13.45±0.56	8.07±0.94	3.03±0.38	0.67±0.18	
^{97}Zr (^{97}Nb)	17.73±0.38	17.24±0.34	14.63±0.31	12.58±0.29	7.36±0.56	3.46±0.13	0.60±0.04	0.18±0.01
^{99}Mo ($^{99}Tc^{m}$)	18.24±0.11	18.24±0.11	14.83±0.34	12.85±0.22	7.18±0.18	3.48±0.09	0.69±0.05	0.25±0.01
^{103}Ru	17.54±1.16	16.37±0.76	13.56±1.25	11.62±0.94	6.69±0.45	3.12±0.18	0.75±0.05	0.13±0.02
^{105}Rh	16.61±0.62	15.97±0.51	13.20±0.98	11.17±0.80	6.24±0.58	2.36±0.18	0.38±0.07	0.11±0.02
^{111}Ag								
^{112}Pd (^{112}Ag)	12.82±0.40	11.53±0.36	8.67±0.34	4.80±0.31	2.81±0.45	1.12±0.11	0.14±0.05	
^{113}Ag	11.71±0.49	10.88±0.78	9.05±0.76	4.91±0.65	2.72±0.69	1.05±0.20		0.03±0.01
^{115}Cd ($^{115}In^{m}$)	10.35±0.31	9.72±0.25	8.10±0.89	4.28±0.96	2.34±0.34	0.96±0.09	0.10±0.04	
$^{117}Cd^{g}$	4.44±0.31	4.53±0.20	3.03±0.20	1.90±0.47	0.78±0.20	0.54±0.16		0.02±0.01
$^{117}Cd^{m}$	4.82±0.61	4.68±0.53	3.06±0.36	1.70±0.69	0.62±0.16	0.27±0.09		
^{126}Sb	7.29±0.47	6.58±0.31	6.04±0.58	2.90±0.58	1.83±0.22	0.71±0.16		
^{127}Sb	9.72±0.60	11.73±0.58	8.52±0.91	5.19±0.47	4.71±0.34	1.65±0.29	0.41±0.16	0.09±0.02
^{128}Sb		5.89±0.20	4.62±0.25	3.19±0.34	2.14±0.27		0.03±0.01	
^{129}Sb	6.80±0.49	3.01±0.13	4.75±0.27	3.43±0.49	2.25±0.49	1.38±0.09	0.24±0.05	0.07±0.01
^{130}I	7.31±0.89	6.13±1.00	6.09±0.71	4.80±0.78				
^{131}I	17.33±0.22	18.82±0.18	14.05±0.29	10.15±0.38	7.16±0.78	3.46±0.18	0.57±0.10	0.17±0.02
^{132}Te (^{132}I)	12.31±0.16	12.71±0.31	7.89±0.56	6.91±0.45	3.79±0.69	1.81±0.11	0.50±0.06	0.18±0.03
^{133}I	10.62±0.36	11.64±0.27	10.62±0.45	7.85±0.51	5.98±0.51	3.10±0.31	0.62±0.07	0.19±0.02
^{135}I (^{135}Xe)	15.47±0.47	15.45±0.11	9.48±0.40	11.04±0.56	7.49±0.42	2.72±0.29	0.61±0.09	0.21±0.03
^{136}Cs	8.21±0.51	8.52±0.20	7.34±0.54	4.95±0.96	2.59±0.18	1.45±0.25	0.19±0.06	
^{139}Ba	12.42±0.38	12.64±0.20	11.48±0.54	8.05±0.94	6.24±0.27	2.92±0.25	0.38±0.07	0.12±0.02
^{140}Ba (^{140}La)	10.10±0.83	10.37±1.00	9.08±0.49	7.18±0.27	4.80±0.69	2.12±0.25	0.44±0.09	
^{141}Ce	10.39±0.56	10.62±0.78	11.71±0.58	8.12±0.78	5.24±0.62	2.25±0.31	0.43±0.09	
^{142}La	7.52±0.49	6.58±0.29	6.18±0.74	5.53±0.45	4.13±0.18	1.63±0.16	0.32±0.05	0.10±0.02
^{143}Ce	8.16±0.51	8.41±0.31	6.27±0.27	4.68±0.20	3.50±0.29	1.85±0.27	0.25±0.07	0.08±0.02
^{149}Nd	2.83±0.22	2.41±0.29	1.96±0.27	1.52±0.34	1.00±0.18	0.69±0.16		
^{151}Pm								
^{153}Sm			0.98±0.11					

ordinary chemical purification, the acid solution was evaporated up on a hot plate, and the residue was dissolved in about 5–10 μl 10M HNO_3, and to it was added about 5–8 ml isopropyl alcohol. Each target material was electrodeposited on a 6-mg/cm^2 Al foil under the condition of 500–800 V, 3–5 mA/cm^2 for 20–30 min while cooling by circulation of water. When the current density became more than 10 mA/cm^2, the deposition efficiency and the quality of the target were deteriorated, and it was necessary to remove the acid by heating. The solution was intermittently stirred by the anode rod attached to a motor for uniform deposition of the target. The efficiency of the electrodeposition was over 80% for all the actinides. The deposition procedure was repeated several times when a thick target was needed. The thickness of each target was determined by α spectrometry to be about 100–300 μg/cm^2 for all elements. The standard sources used for the determination of the target thickness were ^{244}Cm and ^{241}Am purchased from Bureau National de Métrologie (France).

Each target was wrapped with a sheet of Al thick enough for stopping all fission products. Five to eight wrapped targets were stacked for proton bombardment. Several pieces of 10-mg/cm^2 Cu foil were inserted into the target stack at appropriate positions to monitor the beam current. A Faraday cup equipped with a current integrator was used for the measurement of the beam current [8]. An electron suppressor of 300 V/cm was placed between the Faraday cup and the beam collimator for avoiding the secondary electrons. The beam currents were typically 1–2 μA. Their uncertainties were estimated to be about 5–10 %. The proton energy at each target was calculated by use of the range-energy relationship presented by Williamson *et al.* [9] and Northcliffe and Schilling [10]. The beam profile was adjusted to 5 mm i.d. (inner diameter) by a collimator. Targets were bombarded for periods of 30 min to 2 hours to ensure adequate production of fission-product activities. Bombard-

TABLE IV. Fission product yield of the proton-induced fission of ^{235}U.

Fission product	Incident proton energy 18.0 MeV (mb)	15.6 MeV (mb)	14.6 MeV (mb)	13.6 MeV (mb)
^{85}Kr^m	15.99±1.47	7.85±0.74	5.19±0.41	4.38±0.25
^{87}Kr		14.22±0.90	10.51±0.40	6.93±0.21
^{88}Kr	23.20±2.00	12.56±0.44	9.00±0.37	6.08±0.28
^{91}Sr	33.31±2.89	25.94±0.55	19.63±0.68	12.05±0.34
^{92}Sr	33.10±1.61	24.32±1.37	18.51±0.66	12.55±0.51
^{93}Y	34.79±1.44	27.97±0.95	19.61±0.50	11.85±0.39
^{95}Zr		29.93±1.60	23.43±0.61	14.90±0.36
^{97}Zr(^{97}Nb)	48.02±1.68	32.82±1.24	25.59±0.70	8.61±0.30
^{99}Mo (^{99}Tc^m)	46.44±1.48	31.29±0.84	22.48±0.52	15.82±0.55
^{103}Ru	47.16±1.87	30.14±0.80	22.63±0.84	14.59±0.54
^{105}Rh	46.10±2.03	27.34±1.01	19.39±0.76	11.53±0.32
^{111}Ag		14.62±0.88	10.81±0.74	6.72±0.51
^{112}Pd (^{112}Ag)	32.70±4.49	17.33±0.82	10.91±0.49	6.98±0.27
^{113}Ag	34.12±5.01	14.07±0.63	9.78±0.50	5.28±0.37
^{118}Cd (^{118}In^m)	27.03±0.86	12.68±0.65	8.85±0.40	5.17±0.47
^{117}Cd^g	12.79±0.59	6.26±0.59	2.90±0.45	1.32±0.28
^{117}Cd^m	12.46±1.37			
^{128}Sb		7.41±0.71	5.06±0.52	2.44±0.25
^{127}Sb	36.55±1.23	18.35±0.44	14.06±0.32	8.78±0.47
^{128}Sb		8.67±0.90	5.93±0.66	4.01±0.24
^{129}Sb	36.50±2.06	15.23±0.76	9.52±0.72	6.32±0.40
^{130}I		5.48±0.67	3.65±0.45	2.16±0.22
^{131}I	47.58±2.06	29.19±0.99	26.60±0.90	16.85±0.54
^{132}Te (^{132}I)	50.59±3.59	17.07±0.97	13.55±0.62	9.49±0.24
^{133}I	46.19±1.37	29.61±1.05	22.65±0.67	15.90±0.44
^{135}I (^{135}Xe)	52.14±3.59	27.72±0.80	27.86±0.85	18.19±0.79
^{136}Cs		8.61±0.76	6.23±0.65	4.02±0.51
^{139}Ba	38.81±1.05	33.29±1.22	25.16±1.12	18.59±0.95
^{140}Ba (^{140}La)	37.46±1.33	22.81±0.86	17.42±0.43	12.26±0.28
^{141}Ce		21.67±0.95	17.35±0.54	11.75±0.47
^{142}La		23.10±0.67	14.51±0.57	10.20±0.46
^{143}Ce	24.37±1.11	17.07±0.76	14.65±0.49	10.32±0.55
^{149}Nd	13.68±0.83	7.85±0.82	4.35±0.34	2.88±0.49
^{151}Pm		4.03±0.44	3.06±0.30	1.92±0.26
^{153}Sm	6.41±0.44	2.00±0.27	2.13±0.28	1.15±0.12

ments were performed at the tandem accelerator of the Japan Atomic Energy Research Institute (JAERI) and at the cycroton of the Institute for Nuclear Study (INS). The proton energies on the target are listed in Table I together with those of other reaction systems for use in the present discussion.

After the bombardment, γ-ray activities produced in each target-catcher assembly were measured directly with a high-purity Ge detector equipped with a 4096-channel pulse-height analyzer. The produced nuclides were identified with their characteristic γ-ray energies, and their formation cross sections were evaluated from the observed photopeak areas, the target thickness, and from the beam current. Nuclear properties of fission fragments are listed in Table II.

III. RESULTS

Fission-product yields of proton-induced fission of ^{233}U, ^{235}U, ^{236}U, ^{237}Np, ^{239}Pu, ^{242}Pu, ^{244}Pu, ^{241}Am, and ^{243}Am were determined for about 30 fission products in each fissioning system and they are listed in Tables III–XI. The errors cited originate from the consideration of γ-counting statistics and the half-life fitting for the decay of the photopeak area.

A. Mass yield curve

Mass yield curves were constructed from the observed cross section of each fission product to which a correction was applied, when necessary, for the charge distribution by assuming a Gaussian charge distribution with the most probable charge Z_p of unchanged-charge division (UCD) as a first approximation. The most probable charge Z_p for fragment mass number A is given simply by

$$Z_p = \frac{Z_c}{A_c - \nu} A \ , \tag{1}$$

TABLE IV. (*Continued*).

Incident proton energy				
12.5 MeV (mb)	12.0 MeV (mb)	11.4 MeV (mb)	10.2 MeV (mb)	9.0 MeV (mb)
3.01±0.30	2.31±0.06	1.29±0.11	0.41±0.04	0.06±0.02
4.80±0.67	3.84±0.22	2.14±0.22	0.92±0.09	0.12±0.03
4.26±0.46	3.63±0.16	2.07±0.15	0.57±0.03	0.12±0.02
9.43±0.71	5.02±0.12	4.12±0.34	1.60±0.09	0.23±0.04
9.61±0.59	5.47±0.14	4.06±0.24	1.66±0.09	0.26±0.02
10.75±0.76	5.61±0.16	4.92±0.38	2.07±0.20	0.22±0.02
11.22±0.88	6.59±0.49	4.98±0.22	1.95±0.14	0.23±0.02
12.02±0.34	7.53±0.27	5.39±0.32	2.03±0.08	0.27±0.03
11.15±0.57	7.89±0.33	5.43±0.26	1.90±0.13	0.26±0.01
10.01±0.80	5.63±0.16	4.09±0.22	1.58±0.10	0.19±0.02
7.55±0.25	4.14±0.31	2.79±0.31	1.21±0.08	0.16±0.01
4.00±0.46	3.08±0.39	1.72±0.15	0.39±0.04	0.02±0.01
4.02±0.71	2.18±0.27	1.64±0.23	0.41±0.02	0.02±0.01
3.84±0.44	2.33±0.33	1.22±0.14	0.31±0.02	
2.94±0.25	1.73±0.22	1.02±0.09	0.29±0.05	0.01±0.01
1.39±0.30	1.08±0.27	0.54±0.08	0.11±0.02	
			0.05±0.01	
1.48±0.21	0.82±0.06	0.51±0.08	0.17±0.01	
5.73±0.45	3.20±0.29	2.22±0.22	0.75±0.05	0.08±0.02
2.61±0.57	1.26±0.22	0.96±0.47	0.34±0.05	0.03±0.02
4.90±0.79	2.82±0.29	1.99±0.14	0.08±0.02	0.10±0.02
1.97±0.30		0.52±0.09	0.14±0.03	0.04±0.02
12.23±0.74	7.04±0.24	5.01±0.34	1.74±0.14	0.24±0.03
7.00±0.45	4.67±0.22	3.18±0.21	1.31±0.09	0.19±0.02
11.21±0.52	6.20±0.27	4.98±0.22	1.93±0.11	0.27±0.03
13.03±0.46	7.27±0.20	5.54±0.47	1.65±0.12	0.21±0.04
12.58±0.36	1.31±0.29	1.00±0.09	0.34±0.04	0.10±0.01
11.91±0.65	9.57±0.22	5.55±0.32	1.73±0.13	0.85±0.05
8.85±0.46	5.39±0.37	3.90±0.19	1.62±0.08	0.35±0.24
8.36±0.62	5.55±0.31	3.67±0.27	1.57±0.10	0.61±0.20
	4.69±0.35	3.43±0.35	1.40±0.08	0.52±0.22
7.20±0.57	4.28±0.27	3.16±0.20	1.33±0.07	0.66±0.19
2.54±0.34	1.94±0.37	1.21±0.09	0.50±0.05	0.13±0.06
1.68±0.30	1.31±0.27	0.79±0.09	0.27±0.05	
0.55±0.10		0.40±0.06	0.09±0.02	0.20±0.02

TABLE V. Fission product yield of the proton-induced fission of ^{236}U.

Fission product	Incident proton energy 15.6 MeV (mb)	14.8 MeV (mb)	14.0 MeV (mb)	13.1 MeV (mb)	12.1 MeV (mb)	11.2 MeV (mb)	10.2 MeV (mb)	9.0 MeV (mb)
$^{85}Kr^{m}$	6.10±0.84	4.73±0.39	3.95±0.17	2.67±0.15	1.59±0.20	0.78±0.13	0.34±0.04	0.05±0.02
^{87}Kr	11.76±0.61	7.66±0.72	5.71±0.55	4.34±0.19	2.76±0.16	1.39±0.08	0.57±0.05	0.08±0.02
^{88}Kr	12.02±0.74	8.07±0.81	5.80±0.74	4.68±0.23	3.09±0.24	1.55±0.13	0.73±0.05	0.11±0.01
^{91}Sr	23.88±1.27	14.19±0.97	12.30±0.50	8.52±0.44	5.52±0.20	2.60±0.20	1.07±0.07	0.17±0.02
^{92}Sr	22.50±0.90	14.65±0.35	12.74±0.45	8.91±0.27	5.79±0.47	2.80±0.16	1.23±0.09	0.18±0.03
^{93}Y	27.48±0.52	16.85±1.08	14.34±1.24	10.11±0.66	6.85±0.92	3.22±0.28	1.49±0.04	0.33±0.06
^{95}Zr	29.99±1.55	18.39±0.72	15.34±0.97	10.60±1.00	6.85±0.44	3.01±0.26	1.41±0.18	0.25±0.03
^{97}Zr (^{97}Nb)	32.73±1.26	19.88±0.99	16.64±1.33	10.75±0.50	7.30±0.46	3.57±0.19	1.53±0.13	0.21±0.05
^{99}Mo ($^{99}Tc^{m}$)	30.94±1.43	19.49±0.75	20.18±1.18	10.87±0.75	6.76±0.33	3.34±0.22	1.56±0.11	0.22±0.05
^{103}Ru	28.70±1.79	18.26±0.77	14.01±0.86	9.96±0.61	6.10±0.31	2.82±0.17	1.40±0.05	0.15±0.02
^{105}Rh	24.61±1.09	15.36±0.69	12.10±1.18	8.20±0.31	5.79±0.36	2.31±0.21	1.12±0.11	0.11±0.03
^{111}Ag		7.72±1.02	5.16±1.06		1.56±0.28			
^{112}Pd (^{112}Ag)	13.90±1.19	8.26±0.87	5.75±0.77	3.99±0.26	1.92±0.37	0.84±0.17	0.21±0.05	
^{113}Ag	11.35±1.07	7.33±0.48	4.66±0.71	3.46±0.18	1.87±0.20	0.73±0.22		
^{115}Cd ($^{115}In^{m}$)	10.38±0.86	5.23±0.39	4.01±0.53	2.39±0.19	1.30±0.15	0.57±0.14	0.16±0.04	
$^{117}Cd^{g}$	4.86±1.26	2.99±0.78	2.39±0.38	1.23±0.16	0.70±0.21	0.31±0.11	0.05±0.02	
$^{117}Cd^{m}$		1.33±0.19			0.63±0.10			
^{126}Sb	6.40±0.48	2.55±0.26	1.69±0.44	1.12±0.19	0.65±0.14	0.20±0.05		
^{127}Sb	16.68±0.48	10.63±0.58	8.05±0.71	5.43±0.28	3.00±0.22	1.28±0.16	0.48±0.01	
^{128}Sb	7.92±0.36	4.61±0.49	6.61±0.47	2.11±0.16	1.95±0.27	0.57±0.11	0.27±0.01	
^{129}Sb	23.66±1.31		6.55±0.55	4.08±0.06	3.22±0.45	1.38±0.23	0.55±0.11	0.08±0.01
^{130}I	5.02±0.71	2.35±0.25	1.96±0.65		3.03±0.29	0.75±0.15	1.05±0.08	
^{131}I	31.65±1.19	17.91±1.25	15.58±0.93	11.05±0.62	6.27±0.44	3.26±0.22	1.26±0.09	0.14±0.02
^{132}Te (^{132}I)	19.37±0.71	12.45±0.50	10.18±0.65	7.54±0.43	4.76±0.31	2.46±0.19	1.06±0.07	0.17±0.02
^{133}I	29.75±1.43	18.76±0.66	15.96±0.49	10.81±0.67	7.08±0.39	3.68±0.18	1.45±0.06	0.22±0.03
^{135}I (^{135}Xe)	34.75±2.38	19.55±1.97	14.87±0.73	10.34±0.85	6.99±0.30	3.38±0.21	1.41±0.15	0.20±0.04
^{136}Cs	6.38±0.48	3.72±0.25	2.58±0.32	1.73±0.12	1.11±0.22	0.54±0.17		
^{139}Ba	33.32±2.86	19.16±1.04	17.20±0.77	11.37±1.22	7.43±0.47	3.85±0.26	1.72±0.12	0.30±0.05
^{140}Ba (^{140}La)	27.37±2.14	15.17±0.68	12.63±0.84	8.72±0.43	6.01±0.10	3.07±0.16	1.58±0.09	0.26±0.04
^{141}Ce	22.35±0.36	14.09±0.54	11.15±0.65	8.18±0.29	5.07±0.20	2.84±0.22	1.14±0.07	0.17±0.04
^{142}La	19.37±0.95	12.24±0.73	10.77±1.01	7.90±0.27	5.56±0.18	2.63±1.75	1.25±0.11	0.17±0.02
^{143}Ce	18.87±1.19	11.81±0.69	9.62±0.68	7.22±0.43	4.41±0.18	2.37±0.20	1.06±0.08	0.16±0.01
^{149}Nd	5.47±0.67	3.88±0.60	2.79±0.16	2.48±0.23	1.62±0.16	0.96±0.15	0.54±0.07	0.05±0.02
^{151}Pm	4.28±0.95	2.68±0.23	2.88±0.25	1.65±0.16	1.06±0.25	0.49±0.11		
^{153}Sm	2.62±0.48	1.86±0.19	1.65±0.23	1.32±0.13	0.59±0.14	0.29±0.04	0.16±0.04	

TABLE VI. Fission product yield of the proton-induced fission of ^{237}Np.

Fission product	Incident proton energy 31.7 MeV (mb)	28.8 MeV (mb)	27.5 MeV (mb)	26.5 MeV (mb)	25.5 MeV (mb)	24.6 MeV (mb)	23.6 MeV (mb)	22.5 MeV (mb)
^{85}Kr^{m}	11.41±0.57	10.97±0.50	10.58±0.66	9.38±0.83	8.25±0.53	7.19±1.65	6.56±0.18	5.81±0.25
^{87}Kr	16.61±1.66	16.03±0.15	15.92±0.92	15.00±0.98	18.44±1.73	17.24±2.67	19.07±1.64	21.12±1.99
^{88}Kr	16.34±1.29	16.76±0.59	35.65±1.25	16.40±1.79	24.12±1.89	19.43±1.39	16.79±0.73	18.34±0.74
^{91}Sr	39.58±1.29	37.56±1.42	34.78±2.44	34.24±1.58	40.27±1.80	33.62±2.32	38.32±1.92	43.26±1.30
^{92}Sr	28.37±1.84	39.91±1.58	46.37±3.25	34.73±1.34	41.62±1.47	32.73±2.30	39.57±1.98	
^{93}Y	36.14±2.84	38.50±1.24	39.75±1.83	38.25±1.87	46.74±3.62			49.22±2.96
^{95}Zr	55.64±2.00	53.42±2.00	52.40±1.92	49.90±3.08	55.77±3.73	50.23±2.57	53.22±2.58	68.93±2.93
^{97}Zr (^{97}Nb)	68.93±1.22	66.35±1.75	68.88±2.55	69.08±2.32	67.82±2.11	62.02±3.09	63.49±1.92	60.88±2.02
^{99}Mo (^{99}Tc^{m})	38.77±0.70	69.95±2.59	68.07±4.55	70.47±2.25	76.68±1.46	66.23±1.27	34.64±0.76	
^{103}Ru	71.78±3.14	77.91±1.48	74.66±2.44	77.58±2.91	80.65±4.06	74.21±3.34	74.23±1.12	75.86±3.82
^{105}Rh	66.22±2.09	74.00±1.49	81.36±1.80	78.18±1.55	80.09±3.14	69.54±1.46	72.08±2.74	77.30±7.25
^{111}Ag	68.06±2.54	68.70±1.42	67.08±1.75	62.25±2.92	60.02±3.44	50.80±2.89	61.94±3.26	
^{112}Pd (^{112}Ag)	67.06±1.63	67.42±2.11	67.50±2.36	60.34±2.18	67.09±3.55	52.06±2.34	57.86±2.03	51.39±2.26
^{113}Ag	65.60±3.52	66.20±2.66	65.76±1.45	61.67±3.04	56.34±3.15	47.20±3.26	56.48±2.67	47.22±3.50
^{115}Cd (^{115}In^{m})	64.67±1.64	62.71±1.85	61.32±2.98	55.91±1.67	50.77±2.65	42.55±1.28	47.89±1.29	37.74±1.56
^{117}Cd^{g}	19.55±2.77				23.98±0.84	13.29±1.06	12.37±0.94	17.93±2.03
^{117}Cd^{m}	41.31±1.82				28.97±1.98	18.67±1.59		19.06±2.07
^{126}Sb	34.65±1.05	33.66±1.76	30.92±1.73	29.25±1.83	40.07±6.97	53.62±4.34	38.15±6.82	43.84±3.39
^{127}Sb	43.54±3.24	42.85±0.87	40.06±1.62	37.61±0.97	45.75±2.48	56.44±0.93	42.64±0.89	45.09±1.31
^{128}Sb	40.07±2.41	35.88±1.81	37.83±2.18	33.93±1.92	34.28±3.46	42.41±1.76	34.41±2.04	37.59±1.76
^{129}Sb		30.11±1.30	35.59±2.03	26.85±2.33	27.38±1.45	14.70±1.21	19.88±0.98	24.51±1.63
^{130}I	31.19±2.65	28.67±2.55			43.72±3.02			
^{131}I	61.16±1.84	58.91±1.34	60.58±2.33	56.57±2.37	77.17±2.62	65.12±4.79	68.33±3.08	66.16±3.16
^{132}Te (^{132}I)	21.20±1.31	37.16±2.25	43.68±3.12	37.81±1.92	47.05±1.75	34.03±0.78	32.79±3.76	31.56±5.30
^{133}I	39.12±0.93	67.10±2.06	62.43±2.06	59.31±2.61	77.15±2.18	66.13±2.17	55.60±3.00	66.52±1.27
^{135}I (^{135}Xe)	57.94±2.29	64.07±1.41	63.41±3.00	65.72±2.63	67.12±1.64	60.75±1.80	63.28±1.90	67.51±1.69
^{136}Cs	31.47±4.44	34.26±1.86	32.67±2.77	33.17±1.74	46.76±1.43	35.29±1.34	35.06±1.76	
^{139}Ba	53.64±1.08	64.77±2.66	66.94±1.85	60.09±1.55	58.80±6.42	49.04±0.95	52.07±1.34	60.54±1.09
^{140}Ba (^{140}La)	52.56±5.21	58.05±3.07	59.25±3.07	60.38±3.16	56.60±1.98	46.07±0.92	49.37±5.41	51.41±0.97
^{141}Ce	36.56±2.19	41.70±2.25	49.04±2.08	56.32±1.55	45.38±1.34	40.64±1.78	43.56±4.04	38.63±1.76
^{142}La	22.16±1.75	36.44±1.10	41.99±2.60	45.23±2.32	72.55±1.70	28.13±1.74	34.24±1.52	34.57±1.62
^{143}Ce	26.06±0.81	35.42±1.88	37.82±1.28	38.33±1.50	35.74±4.22	31.88±1.25	32.44±0.98	32.50±1.69
^{149}Nd	8.16±0.82	11.42±0.93	12.67±0.90	9.10±0.86	16.16±0.83	13.38±1.46	12.38±0.03	14.00±1.07
^{151}Pm					28.96±1.62			
^{153}Sm		4.22±0.83	3.42±0.17	3.09±0.27				2.01±0.24

TABLE VI. (*Continued*).

Fission product	Incident proton energy 21.6 MeV (mb)	20.5 MeV (mb)	19.5 MeV (mb)	18.5 MeV (mb)	17.5 MeV (mb)	16.5 MeV (mb)	15.5 MeV (mb)	15.1 MeV (mb)
$^{85}Kr^{m}$	5.59±0.20	6.83±0.98	7.77±1.88	8.09±0.20	7.13±1.14	6.16±0.14	5.57±1.16	5.42±0.94
^{87}Kr	20.44±0.90	16.65±1.44	11.91±0.94	19.22±1.04	14.97±1.96	11.59±1.17	10.57±1.29	11.41±0.77
^{88}Kr	16.52±0.62	15.92±0.64	12.65±0.61	18.56±0.90	14.62±0.63	10.99±0.50	12.49±0.99	13.23±0.29
^{91}Sr	34.91±1.47	32.22±1.76	28.24±1.30	30.34±1.12	29.13±1.72	26.66±1.32	21.53±1.10	21.94±0.94
^{92}Sr	32.34±0.92	31.33±1.34	0.415±1.34	29.45±1.34	29.63±1.37	22.41±2.22	23.60±1.44	21.53±0.48
^{93}Y	46.44±1.72	37.67±0.86	34.14±1.50	36.07±2.60	36.56±2.27	32.25±3.68	25.29±2.05	27.17±0.92
^{95}Zr	56.48±2.47	47.43±1.76	37.64±1.86	44.35±1.46	37.75±2.12	33.14±2.41	31.98±1.19	31.76±2.25
^{97}Zr (^{97}Nb)	59.48±1.91	56.99±1.16	51.94±2.38	53.73±2.07	67.40±0.88	41.17±1.61	37.06±1.57	33.60±3.16
^{99}Mo ($^{99}Tc^{m}$)		60.19±2.56	51.24±0.86	58.90±1.82	56.99±0.79	37.38±0.89	45.07±2.89	36.77±2.31
^{103}Ru	68.20±1.50	58.67±1.40	50.99±1.00	61.28±1.34	51.20±1.50	36.16±1.37	41.63±2.03	36.38±2.40
^{105}Rh	63.99±3.33	54.24±0.86	46.07±2.45	50.65±0.90	50.73±1.17	35.76±1.30	33.52±1.61	39.93±2.01
^{111}Ag	42.74±1.16		31.58±1.76	35.64±0.82	32.53±2.24	25.40±2.38	56.46±1.25	
^{112}Pd (^{112}Ag)	39.24±1.23	38.24±3.36	28.91±0.99	35.40±1.05	29.82±1.49	22.83±0.84	20.75±1.12	19.03±1.44
^{113}Ag	36.34±2.73		29.34±1.10	33.19±2.24	30.45±1.92	23.22±2.94	20.52±1.21	15.81±1.20
^{115}Cd ($^{115}In^{m}$)	31.36±1.38	36.59±1.33	26.76±1.66	28.97±0.75	25.25±0.96	17.97±1.30	14.51±1.04	11.79±0.81
$^{117}Cd^{g}$	18.77±1.80	15.65±0.74	11.14±0.92	16.09±1.21	11.78±1.46	12.70±1.01	7.06±1.17	5.66±0.24
$^{117}Cd^{m}$	13.07±1.49	17.42±1.65		14.74±0.34	12.10±1.46	6.40±0.31	4.49±1.19	4.10±0.35
^{126}Sb	29.16±1.81	34.67±1.10	26.81±2.85	37.70±1.88	29.03±5.64	21.61±1.60	19.89±1.25	13.16±2.63
^{127}Sb	37.58±0.75	37.40±3.17	30.32±2.07	34.08±0.58	28.70±1.50	24.19±0.64	25.22±0.78	17.44±1.52
^{128}Sb	34.82±2.42	31.19±1.84	28.66±1.58	27.38±1.58	21.44±2.45	15.94±2.29		16.15±1.62
^{129}Sb	18.29±1.35	19.73±2.36	15.53±0.92	18.63±1.01	19.84±0.92	14.60±2.16	13.55±1.11	10.74±2.94
^{130}I				16.07±2.14	18.99±4.68	11.90±1.87	43.16±4.32	
^{131}I	58.24±0.83	63.59±1.67	51.19±4.19	58.86±1.48	48.53±6.35	49.47±1.86	39.39±1.54	36.81±2.30
^{132}Te (^{132}I)	30.65±1.97	31.90±4.45	35.87±1.01	31.88±1.54	43.66±1.11	26.64±0.96	31.91±1.18	27.69±2.71
^{133}I	59.23±1.48	54.27±3.19	48.95±0.95	51.67±0.83	51.85±1.55	42.47±2.52	44.78±2.11	35.26±2.29
^{135}I (^{135}Xe)	63.69±1.46	56.91±2.20	49.34±0.71	53.60±1.31	54.68±2.36	43.83±0.88	36.21±0.87	38.52±1.65
^{136}Cs	11.16±2.16	19.52±1.85	44.12±4.06	34.01±2.12	23.71±0.74	22.16±0.91	20.52±3.71	16.78±1.23
^{139}Ba	46.95±1.27	48.50±2.24	39.07±0.03	37.91±1.23	38.95±1.28	35.69±0.27	36.49±2.57	33.62±1.54
^{140}Ba (^{140}La)	42.57±1.32	45.59±0.92	41.43±2.39	39.88±1.72	38.90±1.17	34.17±1.23	35.92±2.22	31.57±1.58
^{141}Ce	37.50±2.39	41.02±2.60	30.98±0.61	33.01±1.01	32.40±1.98	25.03±2.58	28.88±1.01	
^{142}La	32.00±1.54	29.89±1.70	28.28±1.42	28.50±2.04	28.60±1.42	21.54±0.92	26.44±1.49	27.98±1.88
^{143}Ce	31.83±0.95	30.08±1.04	24.11±1.25	29.58±1.25	29.54±1.77	22.64±1.45	26.25±1.19	21.41±0.83
^{149}Nd	12.41±0.83	11.52±0.91	11.12±2.36	11.32±0.87	9.264±0.60	9.253±0.43	10.00±0.86	9.61±0.67
^{151}Pm							6.38±0.61	
^{153}Sm	2.02±0.27		2.26±0.91			1.25±0.09		

TABLE VI. (*Continued*)

Fission product	Incident proton energy 15.0 MeV (mb)	14.7 MeV (mb)	14.4 MeV (mb)	14.2 MeV (mb)	13.7 MeV (mb)	13.6 MeV (mb)	13.2 MeV (mb)	12.8 MeV (mb)
$^{85}Kr^{m}$	6.11±1.14	5.66±1.63	4.51±0.38	5.70±0.27	4.26±0.32	4.19±0.33	3.94±1.35	3.26±0.66
^{87}Kr	10.79±0.80	8.49±0.47		8.40±1.82		8.45±2.13	5.37±0.36	4.21±0.38
^{88}Kr	10.25±1.18	7.914±0.90	8.44±0.66	8.26±0.62	7.23±0.53	7.29±0.40	5.48±0.69	4.58±0.69
^{91}Sr	20.63±1.14	21.37±1.78	15.98±0.42	15.98±0.38	13.14±0.79	15.20±1.84	11.87±0.34	8.61±0.59
^{92}Sr	18.85±1.12	16.43±1.87	15.40±0.99	16.58±1.08	11.16±0.73	14.46±0.83	10.71±0.84	8.31±1.58
^{93}Y	25.98±1.90	22.23±2.20		13.89±0.24	12.17±0.42	17.81±1.16	15.72±1.05	10.77±0.66
^{95}Zr	30.24±1.43	25.28±0.88		21.34±1.00	16.82±0.35	18.11±0.42	16.28±1.56	13.23±0.81
^{97}Zr (^{97}Nb)	32.63±0.83	30.91±1.83	24.07±1.44	23.84±1.40	18.82±1.64	24.68±0.89	20.51±1.11	17.84±0.67
^{99}Mo ($^{99}Tc^{m}$)	33.84±1.66	28.96±1.51	26.57±1.26	23.00±0.83	22.58±1.99	26.28±0.79	17.09±2.41	13.48±0.77
^{103}Ru	40.36±1.39	33.98±1.06	25.40±1.91	28.21±1.46	24.34±1.56	28.92±0.86	21.28±1.12	16.22±1.12
^{105}Rh	30.17±1.43	28.67±0.71	31.76±1.25	24.99±1.30	26.33±1.58	24.08±0.81	18.74±1.19	16.08±0.92
^{111}Ag	18.66±1.76							
^{112}Pd (^{112}Ag)	16.64±0.84	16.07±1.08	13.42±1.47	10.76±1.09	10.39±1.26	10.28±1.08	9.34±0.64	6.56±0.76
^{113}Ag	17.39±1.67	14.99±1.07	11.41±0.78	10.35±0.99	6.89±0.93	8.29±0.76	9.38±0.41	5.81±0.98
^{115}Cd ($^{115}In^{m}$)	11.53±0.74	9.38±1.75	8.34±0.65	7.04±1.66	5.84±0.42	8.76±0.71	6.05±0.51	4.16±0.37
$^{117}Cd^{g}$	3.97±0.52	4.10±1.44	3.84±0.26	2.21±0.51		2.48±0.29	3.52±0.21	1.75±0.38
$^{117}Cd^{m}$	4.58±0.20	3.65±0.34	3.41±0.32	1.90±0.62		2.06±0.19	1.92±0.35	0.71±0.10
^{126}Sb	9.79±1.04	8.74±1.04	11.97±1.58	6.58±1.41		6.35±0.81	4.78±0.63	4.34±0.63
^{127}Sb	18.44±0.68	14.03±0.68	13.01±1.45	11.68±1.07	13.83±1.37	11.45±0.74	8.50±1.54	5.81±0.42
^{128}Sb		11.33±2.05	11.31±1.24	8.42±0.92	10.82±1.43	8.57±1.37	8.03±0.66	4.69±0.63
^{129}Sb	17.28±1.60	10.53±1.53	8.29±1.40	7.17±1.75		6.38±0.75	4.94±0.12	
^{130}I	10.58±2.20	7.37±1.08		4.92±0.66		5.70±1.52	4.96±0.75	3.14±0.75
^{131}I	36.84±0.94	34.17±1.56	32.85±1.79	24.08±1.84	27.41±1.91	26.13±1.37	16.38±1.08	18.99±1.07
^{132}Te (^{132}I)		28.97±1.61	24.28±2.06	19.41±1.10	15.74±2.25	19.05±0.82	14.97±1.80	9.74±0.67
^{133}I	35.98±2.21	29.54±1.87	26.69±0.81	22.52±1.64	21.71±0.82	25.55±0.61	16.23±0.92	14.64±1.15
^{135}I (^{135}Xe)	28.34±2.66	32.52±1.64	28.82±1.69	21.51±1.00	22.54±1.92	19.46±0.92	17.21±1.42	13.32±1.42
^{136}Cs	13.92±0.92	18.46±0.95	12.16±0.34	11.99±1.64	9.36±0.41	7.672±0.36	6.41±0.12	5.18±0.58
^{139}Ba	29.31±2.41	29.52±0.69	26.71±0.11	19.10±1.50	17.55±2.07	21.86±1.24	15.80±1.58	13.72±1.86
^{140}Ba (^{140}La)	29.12±2.42	22.49±1.67	23.40±3.72	19.70±1.84	18.68±1.42	17.97±1.57	13.38±1.60	11.97±1.96
^{141}Ce	22.33±1.01	23.84±1.21		15.62±0.91		15.28±1.04		12.17±0.50
^{142}La	20.39±1.88	19.00±0.68		15.70±1.10		13.80±2.24	9.44±0.77	8.60±1.35
^{143}Ce	17.03±2.21	15.96±1.79	15.75±1.34	13.82±0.68	11.91±0.83	14.29±1.79	10.85±1.84	9.20±1.80
^{149}Nd	7.48±0.36	4.75±0.97	5.68±0.40	4.53±0.99	4.25±0.51	5.58±0.26	2.96±0.62	3.30±0.45
^{151}Pm		3.28±0.70		2.50±0.30		2.75±1.66		
^{153}Sm		0.99±0.16		0.75±0.66			1.26±0.11	0.80±0.32

TABLE VI. (*Continued*).

Fission product	Incident proton energy 12.6 MeV (mb)	11.9 MeV (mb)	11.2 MeV (mb)	10.8 MeV (mb)	10.2 MeV (mb)	9.8 MeV (mb)
$^{85}Kr^{m}$	3.17±0.27	2.21±0.34	1.46±0.26	1.49±0.22	0.65±0.08	0.66±0.09
^{87}Kr	4.89±0.32	2.89±0.72	1.91±0.27	1.69±0.17	0.92±0.42	
^{88}Kr	5.40±0.67	3.08±0.38	2.63±0.20	1.94±0.48	1.16±0.32	1.25±0.18
^{91}Sr	7.21±0.16	6.38±0.66	4.22±0.32	3.80±0.40	1.51±0.20	1.58±0.26
^{92}Sr	8.44±0.58	5.93±1.05	4.16±0.36	3.80±0.71	1.84±0.25	1.85±0.40
^{93}Y	10.16±0.83	8.10±0.82	4.45±0.90	4.30±0.63	2.09±0.20	
^{95}Zr	13.07±0.66	9.05±0.32	6.61±0.55	5.92±0.74	2.52±0.23	2.53±0.30
^{97}Zr (^{97}Nb)	15.53±0.92	10.26±0.81	7.22±0.80	6.61±0.79	3.16±0.17	3.26±0.66
^{99}Mo ($^{99}Tc^{m}$)	15.00±0.82	11.65±0.67	8.10±0.25	6.21±1.26	3.90±0.27	4.10±0.69
^{103}Ru	16.15±0.96	11.71±0.24	7.42±0.44	6.69±0.69	3.39±0.21	3.02±0.23
^{105}Ru	16.16±0.51	9.91±0.33	7.52±0.29	8.03±0.47	3.20±0.13	3.09±0.67
^{111}Ag		5.14±0.19				
^{112}Pd (^{112}Ag)	6.98±1.06	4.34±0.44	1.81±0.26	1.64±0.53	0.73±0.09	0.53±0.19
^{113}Ag	6.84±0.42	3.80±1.12	1.46±0.14	1.28±0.99	0.53±0.08	
^{115}Cd ($^{115}In^{m}$)	3.89±0.55	2.53±0.35	1.01±0.18	0.92±0.26	0.30±0.15	0.04±0.01
$^{117}Cd^{g}$	1.77±0.19	1.48±0.22		0.42±0.24		
$^{117}Cd^{m}$	0.94±0.13	0.46±0.20	0.32±0.12			
^{126}Sb		3.27±0.67		1.53±0.23		
^{127}Sb	6.48±1.17	4.54±0.48	2.56±0.42	2.73±0.38	2.09±0.33	1.13±0.24
^{128}Sb		3.41±0.92	1.69±0.32	1.31±0.27		0.59±0.18
^{129}Sb	3.41±0.82	2.15±0.42			1.29±0.22	0.83±0.26
^{130}I		2.08±0.24				
^{131}I	13.16±0.29	10.28±1.08	7.02±0.41	6.85±0.82	3.40±0.31	3.13±0.28
^{132}Te (^{132}I)	8.78±1.16	6.83±0.98	4.05±0.37	6.11±0.92	1.97±0.24	1.76±0.46
^{133}I	15.81±2.11	9.75±0.66	9.08±0.68	6.42±0.43	3.39±0.20	2.55±0.22
^{135}I (^{135}Xe)	13.88±0.68	7.58±0.64	8.61±0.23	5.94±0.61	3.20±0.16	1.81±0.27
^{136}Cs	3.44±0.52	3.46±0.59	1.92±0.22	1.74±0.40	0.48±0.17	
^{139}Ba	11.58±1.49	7.19±0.98	6.19±0.94	5.97±0.67	2.78±0.16	2.84±0.30
^{140}Ba (^{140}La)	11.60±0.74	6.91±0.24	5.96±0.28	5.59±0.30		2.38±0.20
^{141}Ce	10.93±0.12		4.75±0.98		2.63±0.62	
^{142}La		6.05±0.93		4.67±0.69		
^{143}Ce	10.23±1.73	6.23±1.42	4.28±0.50	3.47±0.17	1.61±0.12	1.63±0.22
^{149}Nd	3.32±0.40	2.22±0.65	1.17±0.19	1.17±0.25	0.53±0.17	0.25±0.09
^{151}Pm						
^{153}Sm		0.91±0.49				

TABLE VII. Fission product yield of the proton-induced fission of ^{239}Pu.

Fission product	Incident proton energy 15.5 MeV (mb)	14.6 MeV (mb)	13.9 MeV (mb)	13.0 MeV (mb)	12.2 MeV (mb)	11.2 MeV (mb)	9.8 MeV (mb)
$^{85}Kr^{m}$	3.66±0.20	3.44±0.13	2.30±0.13	1.36±0.11	0.89±0.07	0.26±0.11	
^{87}Kr	4.29±0.39	4.18±0.31	4.27±1.31	1.82±0.15	1.12±0.15	0.33±0.09	
^{88}Kr	4.82±0.37	4.51±0.44	3.31±0.37	2.08±0.33	1.29±0.20	0.48±0.13	
^{91}Sr	7.82±1.25	8.85±0.81	6.18±0.24	4.20±0.31	2.96±0.42	0.70±0.20	0.15±0.02
^{92}Sr	8.85±0.33	8.58±0.22	4.14±0.44	4.31±0.68	2.83±0.22	0.79±0.04	
^{93}Y		10.10±0.59	8.02±1.53	5.06±0.22	3.55±0.53	1.12±0.20	0.11±0.04
^{95}Zr	12.88±1.73	12.72±0.28	10.51±1.55	7.38±0.94	5.34±0.20	1.36±0.18	
^{97}Zr (^{97}Nb)	16.47±0.33	15.29±0.59	11.98±0.22	8.91±0.33	5.98±0.22	2.03±0.22	0.24±0.07
^{99}Mo ($^{99}Tc^{m}$)	19.51±0.20	17.72±0.13	13.01±0.20	9.96±0.24	6.61±0.11	2.63±0.09	0.35±0.09
^{103}Ru	20.04±0.35	18.75±0.50	13.56±1.75	11.17±0.28	7.14±1.23	2.08±0.50	0.33±0.11
^{105}Rh	21.75±0.92	19.49±0.42	13.49±0.68	10.10±0.44	7.38±0.48	2.58±0.50	0.61±0.11
^{111}Ag	14.98±0.33				2.74±0.77		
^{112}Pd (^{112}Ag)	13.01±0.50	10.62±0.48	6.85±0.37	3.83±0.46	2.32±0.26	0.57±0.13	0.07±0.06
^{113}Ag	11.91±1.95	8.85±1.12	6.11±1.05	3.72±0.50	1.97±0.35		
^{115}Cd ($^{115}In^{m}$)	9.31±0.48	7.69±0.33	4.93±0.53	2.67±0.55	1.14±0.28	0.31±0.11	
$^{117}Cd^{g}$	3.64±0.46	2.74±0.48	2.04±0.37	0.92±0.18	0.28±0.15		
$^{117}Cd^{m}$	4.05±0.65	3.82±0.44	2.83±0.33	0.82±0.22	0.15±0.05	0.35±0.15	
^{126}Sb	5.72±0.57	4.82±0.48	3.79±0.66	1.64±0.15	1.10±0.20		
^{127}Sb	12.20±1.20	10.34±1.27	7.64±1.40	4.60±0.13	3.26±0.57	0.72±0.18	
^{128}Sb	4.20±0.37	5.30±0.26		1.86±0.24			
^{129}Sb	4.80±0.85	5.93±0.13	3.48±0.42	1.91±0.33	1.77±0.20		
^{130}I	10.03±0.28				2.67±0.59		
^{131}I	19.03±0.53	18.31±0.48	14.17±1.07	8.41±0.92	6.48±0.24	1.34±0.31	0.39±0.11
^{132}Te (^{132}I)	12.96±0.57	14.41±0.39	9.68±0.66	5.37±0.50	5.08±0.39	1.05±0.07	
^{133}I	13.05±0.44	12.61±0.22	10.05±0.37	7.38±0.77	6.29±0.20	2.53±0.20	
^{135}I (^{135}Xe)	19.29±1.66	18.07±1.03	12.53±0.37	9.35±0.55	7.12±0.31	2.45±0.39	0.35±0.11
^{135}Cs	10.51±1.27	8.41±0.79	5.56±0.48	2.30±0.22	2.65±0.31	0.50±0.20	
^{139}Ba	14.32±0.99	12.72±0.37	9.83±0.85	7.47±0.28	5.37±1.31	1.65±0.60	
^{140}Ba (^{140}La)	12.05±0.24	11.28±0.85	9.48±0.44	7.82±0.33	5.39±0.77	1.51±0.18	0.22±0.09
^{141}Ca	11.69±2.67		8.96±1.69	6.90±1.42	4.88±0.44	1.55±0.31	
^{142}La	9.86±0.53	8.65±0.70	6.75±0.90	5.15±0.79	3.31±0.66	0.99±0.24	
^{143}Ce	8.85±0.44	9.42±0.26	6.90±0.33	4.49±0.46	3.20±0.31	1.01±0.15	0.18±0.09
^{149}Nd	3.61±0.59	3.22±0.26	2.45±0.46	1.86±0.22	1.23±0.22	0.26±0.13	
^{151}Pm	3.39±0.74	2.26±0.24	2.21±0.57				
^{153}Sm							

where Z_c and A_c are the charge and the mass of fissioning nuclide, ν is the number of prefission neutrons. The ν was estimated with statistical model calculations [11]. The Gaussian width parameter of 0.95 was used as suggested by McHugh *et al.* [12] The corrections were the largest for the $^{233}U+p$ system and the smallest for the $^{244}Pu+p$ system in the present work due to the charge density of the compound nucleus. For the fission of $^{233}U+p$, for example, the correction was 5.1%, 15.6%, 35.5%, 47.5%, and 8.8% for ^{127}Sb, ^{128}Sb, ^{129}Sb, ^{132}Te, and ^{135}Xe, respectively, with an assumption of only the first-chance fission.

In order to show how the mass yield curve varies as a function of the proton energy, a three-dimensional figure is plotted in Fig. 1 for the $^{237}Np+p$. To draw a smooth mass yield curve through the data points, so-called mirror points were also used. They were obtained by folding the plotted data points at an appropriate symmetric mass

TABLE VIII. Fission product yield of the proton-induced fission of ^{242}Pu.

Fission product	Incident proton energy 12.0 MeV (mb)	18.0 MeV (mb)
$^{85}Kr^m$	3.31±0.07	1.23±0.07
^{87}Kr	5.53±0.09	1.44±0.13
^{88}Kr	6.85±0.10	1.41±0.18
^{91}Sr	8.11±0.41	2.56±0.46
^{92}Sr		2.82±0.63
^{93}Y	11.18±0.05	3.22±0.48
^{95}Zr	12.73±0.78	5.97±1.78
^{97}Zr (^{97}Nb)	17.71±1.15	5.93±0.92
^{99}Mo ($^{99}Tc^m$)	26.90±0.95	6.73±1.11
^{103}Ru	29.34±1.05	8.39±0.44
^{105}Rh	32.25±1.15	9.10±0.32
^{111}Ag		
^{112}Pd(^{112}Ag)	18.22±0.69	2.12±0.75
^{113}Ag	19.13±0.51	2.55±0.17
^{115}Cd ($^{115}In^m$)	11.56±0.44	1.42±0.21
$^{117}Cd^g$	7.71±0.16	0.96±0.13
$^{117}Cd^m$		
^{126}Sb		
^{127}Sb	9.50±0.59	2.46±0.08
^{128}Sb		
^{129}Sb	16.25±1.28	2.28±0.12
^{130}I		4.63±0.17
^{131}I	18.78±0.58	4.38±0.21
^{132}Te (^{132}I)	22.26±0.80	3.33±0.11
^{133}I	28.68±0.94	6.06±0.29
^{135}I (^{135}Xe)	24.55±0.80	6.64±0.32
^{136}Cs	5.05±0.40	
^{139}Ba	26.18±1.08	8.16±0.24
^{140}Ba (^{140}La)	23.91±0.97	6.66±0.15
^{141}Ce	18.28±0.51	7.05±0.26
^{142}La		4.21±0.07
^{143}Ce	16.85±0.53	3.02±0.20
^{149}Nd	9.48±0.12	2.02±0.18
^{151}Pm		1.26±0.22
^{153}Sm	2.66±0.61	1.12±0.09

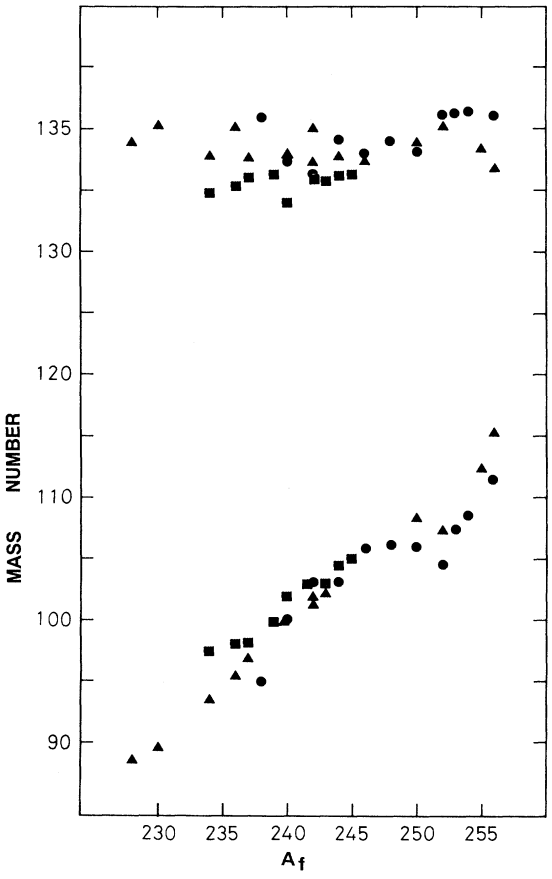

FIG. 3. Weighted mean peak position of light and heavy asymmetric peaks in spontaneous fissions (●), thermal-neutron-induced fissions (▲) and proton-induced fissions for the excitation energy of 16 MeV (■).

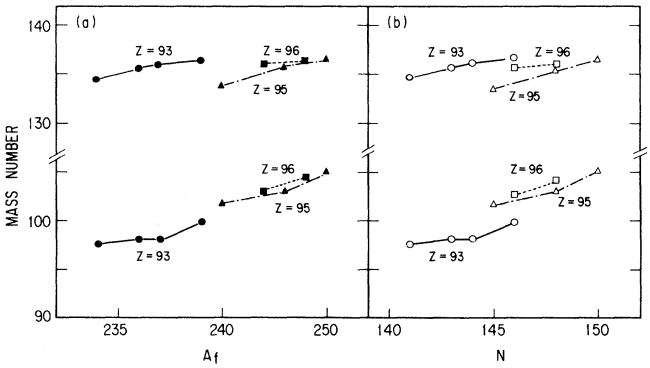

FIG. 4. Isotropic trend of the weighted mean mass of the light and heavy asymmetric peaks as a function of (a) the compound mass number (closed symbols) and (b) the neutron number (open symbols).

TABLE IX. Fission product yield of the proton-induced fission of ^{244}Pu.

Fission product	Incident proton energy 18.0 MeV (mb)	15.6 MeV (mb)	14.4 MeV (mb)	13.1 MeV (mb)	12.0 MeV (mb)	11.7 MeV (mb)	10.2 MeV (mb)
^{85}Kr^{m}	3.88±0.31	2.72±0.50	1.75±0.38	1.28±0.96	0.88±0.12	0.64±0.12	0.20±0.03
^{87}Kr	6.19±0.50	2.86±0.68	1.46±0.95	1.28±0.95	1.30±0.13	0.35±0.11	
^{88}Kr	5.68±0.45	3.91±0.28	3.07±1.36	2.10±0.56	1.66±0.13	1.49±0.25	
^{91}Sr	12.61±1.01	6.48±0.47	6.25±1.59	4.09±0.47	2.71±1.71	2.37±0.31	
^{92}Sr	12.10±0.97	7.42±0.53	5.46±1.73	3.85±0.36	2.56±0.13	2.01±0.36	0.85±0.13
^{93}Y	14.08±0.70	8.44±0.61	8.32±2.14	5.17±0.88			
^{95}Zr	17.74±0.89	12.64±0.91	9.49±3.39	7.74±0.80			
^{97}Zr (^{97}Nb)	22.80±1.14	14.60±1.05	11.21±0.70	7.91±0.93	4.97±0.17	5.93±0.53	1.34±0.20
^{99}Mo (^{99}Tc^{m})	33.37±1.67	20.15±1.45	15.83±1.52	11.50±1.96	7.68±0.80	7.88±0.71	2.10±0.32
^{103}Ru	38.21±1.91	24.15±1.74	19.45±1.11	13.11±1.37	8.45±0.50	7.94±0.73	2.48±0.37
^{105}Rh	47.37±2.37	23.36±4.85	23.94±1.75	16.59±2.26	12.99±0.72	10.07±0.91	1.90±0.28
^{111}Ag			14.40±2.40		7.14±0.65		
^{112}Pd (^{112}Ag)	35.14±2.11	12.88±0.93	10.37±1.50	7.04±1.81	4.27±0.47	3.68±0.33	0.85±0.13
^{113}Ag	31.74±1.90	16.44±1.18	7.15±1.63	5.66±1.46	3.24±0.43	±	
^{115}Cd (^{115}In^{m})	27.48±1.65	7.56±0.54	5.20±1.41	3.94±1.01	2.02±0.54	1.46±0.55	0.29±0.06
^{117}Cd^{g}	12.31±0.74		1.66±0.55				
^{117}Cd^{m}	9.75±0.59		2.16±1.28				
^{126}Sb	15.85±0.95		2.25±0.76		2.72±0.19		
^{127}Sb	22.12±1.33	10.34±0.74	7.12±1.24	3.53±0.91	2.84±0.27	3.53±0.33	0.32±0.06
^{128}Sb		3.15±0.23	2.31±0.90	1.46±0.38			1.06±0.15
^{129}Sb	33.39±2.00	8.15±0.59	7.33±0.64	4.41±1.13	2.96±0.27		
^{130}I			18.51±0.91	8.03±2.06			6.13±0.93
^{131}I	40.71±2.44	20.35±1.47	13.29±2.30	10.66±1.74	8.11±0.22	5.99±0.38	1.66±0.27
^{132}Te (^{132}I)	43.63±2.62	17.32±3.07	11.80±3.18	10.13±2.60	12.28±0.77	5.29±0.36	1.73±0.27
^{133}I	41.43±2.49	20.21±1.45	15.65±2.79	11.13±0.86	3.78±0.46	5.26±0.46	4.09±0.63
^{135}I (^{135}Xe)	47.37±3.32	22.63±2.86	17.75±3.20	12.12±1.11	9.16±0.25	5.84±0.38	1.49±0.24
^{136}Cs							
^{139}Ba	39.47±2.76	21.14±1.52	20.12±4.20	14.57±1.74	10.28±0.28	5.40±0.37	1.87±0.30
^{140}Ba (^{140}La)	30.72±2.15	20.41±1.47		9.93±0.55	8.26±0.37	8.70±0.67	3.74±0.58
^{141}Ce	23.82±1.67	19.10±1.37	14.42±1.69	10.72±1.75	7.53±0.47	5.02±0.35	2.37±0.36
^{142}La	28.14±1.97	12.76±0.92	9.62±2.42	7.04±0.81	5.88±0.27	3.83±0.32	1.05±0.15
^{143}Ce	25.31±1.77	14.02±1.01	9.81±3.28	8.26±0.52	5.60±0.38	3.85±0.42	1.52±0.24
^{149}Nd	11.37±2.48	5.69±0.41	4.56±0.98	3.47±0.89	2.94±0.19	2.77±0.39	0.58±0.09
^{151}Pm				2.80±0.72			
^{153}Sm	5.98±2.35		2.19±0.44		1.62±0.24		

TABLE X. Fission product yield of the proton-induced fission of ^{241}Am.

Fission product	Incident proton energy 16.0 MeV (mb)	15.0 MeV (mb)	14.0 MeV (mb)	13.7 MeV (mb)	12.0 MeV (mb)	11.0 MeV (mb)	10.0 MeV (mb)	9.0 MeV (mb)
$^{85}Kr^{m}$	1.60±0.13	1.66±0.13	1.64±0.13	1.33±0.11	1.25±0.10	0.62±0.05	0.24±0.02	0.08±0.01
^{87}Kr	2.83±0.23	2.14±0.17	4.07±0.33	3.44±0.27	2.80±0.22	1.43±0.11	0.47±0.04	
^{88}Kr	3.88±0.31	2.58±0.21	5.81±0.46	4.52±0.36	2.47±0.20	1.04±0.08		
^{91}Sr	11.78±0.94	9.39±0.75	6.79±0.54	6.80±0.54	3.83±0.31	1.82±0.15	1.06±0.08	0.33±0.03
^{92}Sr	14.87±1.19	10.24±0.82	7.40±0.59	6.62±0.53	5.13±0.41	1.69±0.14	0.92±0.07	0.28±0.02
^{93}Y	13.20±1.06	12.87±1.03	9.17±0.73	9.36±0.75			0.96±0.08	
^{95}Zr				12.06±0.96				
^{97}Zr (^{97}Nb)	23.01±1.84	18.21±1.46	15.47±1.24	15.54±1.24	6.85±0.55	2.86±0.23	1.45±0.12	0.68±0.05
^{99}Mo ($^{99}Tc^{m}$)	33.19±2.66	22.92±1.83	18.94±1.52	20.22±1.62	7.25±0.58	2.73±0.22	1.06±0.08	0.42±0.03
^{103}Ru	29.80±2.38	29.26±2.34	17.24±1.38	21.49±1.72	10.38±0.83	3.64±0.29	1.65±0.13	0.62±0.05
^{105}Rh	37.76±3.02	27.84±2.23	20.02±1.60	23.02±1.84	11.00±0.88	4.03±0.32	1.52±0.12	0.73±0.06
^{111}Ag		15.16±1.21		11.32±0.91				
^{112}Pd (^{112}Ag)	18.76±1.50	17.29±1.38	6.44±0.52	10.26±0.82	3.58±0.29	1.04±0.08	0.38±0.03	0.05±0.00
^{113}Ag	19.62±1.57	12.70±1.02	6.98±0.56		2.88±0.23			
^{115}cd ($^{115}In^{m}$)	12.28±0.98	10.97±0.88	6.04±0.48	6.55±0.52	2.15±0.17	0.52±0.04	0.17±0.01	
$^{117}Cd^{g}$		4.11±0.33	2.35±0.19	1.24±0.10	1.18±0.09			
$^{117}Cd^{m}$				1.08±0.09				
^{126}Sb	8.14±0.65			6.54±0.52				
^{127}Sb	16.04±1.28	14.73±1.18	5.29±0.42	7.13±0.57	4.55±0.36	0.98±0.08		0.11±0.01
^{128}Sb	9.19±0.74	7.13±0.57	3.69±0.30					
^{129}Sb								
^{130}I								
^{131}I	16.60±1.33	14.47±1.16	9.84±0.79	17.95±1.44	8.03±0.64	2.99±0.24	0.79±0.06	0.36±0.03
^{132}Te (^{132}I)	23.69±1.90	19.99±1.60	13.62±1.09	9.73±0.78	2.88±0.23	1.43±0.11		0.31±0.02
^{133}I	24.68±1.97	23.39±1.87	11.95±0.96	22.40±1.79	6.15±0.49	2.34±0.19	1.06±0.08	0.62±0.05
^{135}I (^{135}Xe)	22.71±1.82	20.02±1.60	13.69±1.10	23.80±1.90	7.45±0.60	2.99±0.24	1.45±0.12	0.60±0.05
^{136}Cs	10.86±0.87	10.06±0.80	3.19±0.25		1.41±0.11			
^{139}Ba	29.92±2.39	27.12±2.17	17.99±1.44	22.59±1.81	8.25±0.66	4.55±0.36	1.39±0.11	0.42±0.03
^{140}Ba (^{140}La)	30.91±2.47	24.32±1.95	23.27±1.86	18.66±1.49	9.05±0.72	3.25±0.26	1.72±0.14	0.31±0.02
^{141}Ce	31.96±2.56	12.74±1.02	7.25±0.58	18.84±1.51	3.00±0.24	3.12±0.25		0.60±0.05
^{142}La	28.69±2.30	15.94±1.28	10.36±0.83	16.39±1.31	5.38±0.43	2.73±0.22	0.92±0.07	
^{143}Ce	19.93±1.59	13.30±1.06	14.06±1.12	12.13±0.97	4.40±0.35	2.47±0.20	0.96±0.08	0.49±0.04
^{149}Nd	4.45±0.36	2.92±0.23	4.18±0.33	6.48±0.52	2.25±0.18	1.04±0.08	0.42±0.03	0.16±0.01
^{151}Pm	5.45±0.44	2.22±0.18		5.21±0.42				
^{153}Sm	2.04±0.16			2.46±0.20				

number which was a few masses smaller than the half of the compound mass number. The uncertainty of each datum point is not shown in the figure, but it is given in Table VI.

B. Fission cross section

Fission cross sections (σ_{fission}) were obtained by normalizing the area under the mass yield curve to 200%. They are shown in Figs. 2(a)–2(c) as a function of proton energy. The uncertainty of each datum point is estimated to be as large as 30% due to the errors involved in the determination of the target amount and the intensity of the proton beam in addition to those involved in the determination of each mass-chain yield. In the threshold region of the excitation function, the error of the proton energy can be as large as 1 MeV because of the stacked target method used in the present work. Fission cross sections in proton-induced reactions have been only reported in literature for $^{233}U+p$ and $^{238}U+p$, $^{232}Th+p$ and $^{238}U+p$, by Bate *et al.* [13], Kononov *et al.* [14], and Choppin *et al.* [15], respectively, and for $^{237}Np+p$ by Polak *et al.* [16]. The present results for $^{233}U+p$ and $^{237}Np+p$ are in agreement with those literature values within the cited errors.

IV. DISCUSSION

The mass yield curves obtained are asymmetric as expected, and the relative height of the valley region depends strongly on the incident proton energy. But details of the shapes of asymmetric peaks are different from each other. Gross features of mass yield curves are discussed in the following in terms of the weighted mean mass, the full width at half maximum (FWHM) of the asymmetric

TABLE XI. Fission product yield of the proton-induced fission of ^{243}Am.

Fission product	Incident proton energy 15.6 MeV (mb)	14.0 MeV (mb)	12.0 MeV (mb)	10.4 MeV (mb)
$^{85}Kr^{m}$	2.65±0.33	1.29±0.20	1.21±0.23	0.17±0.04
^{87}Kr	3.53±0.39	2.10±0.30		0.26±0.05
^{88}Kr				
^{91}Sr	8.70±0.57	4.15±0.47	2.46±0.16	0.62±0.08
^{92}Sr	8.24±0.40	4.32±0.48	2.75±0.22	0.60±0.07
^{93}Y	13.36±0.65	5.60±0.56	3.62±0.49	0.75±0.10
^{95}Zr				
^{97}Zr (^{97}Nb)	15.82±1.57	7.06±0.49	5.21±0.33	0.95±0.12
^{99}Mo ($^{99}Tc^{m}$)	15.96±1.54	8.24±0.63	6.16±0.31	1.25±0.12
^{103}Ru	20.51±1.67	10.71±0.58	7.22±0.42	1.60±0.16
^{105}Rh	19.89±2.71	9.55±0.58	8.50±0.59	1.45±0.18
^{111}Ag				
^{112}Pd (^{112}Ag)	9.52±1.09	4.44±0.51	2.18±0.32	0.30±0.10
^{113}Ag	7.40±1.19	4.36±0.34	1.66±0.36	
^{115}Cd ($^{115}In^{m}$)	5.25±0.99	2.40±0.40	1.30±0.35	0.14±0.10
$^{117}Cd^{g}$				
$^{117}Cd^{m}$				
^{126}Sb				
^{137}Sb	5.63±0.79	2.45±0.45	1.55±0.49	0.24±0.06
^{128}Sb				
^{129}Sb	7.59±0.12	2.85±0.31	2.31±0.57	0.30±0.10
^{130}I				
^{131}I				0.95±0.15
^{132}Te (^{132}I)	12.53±1.86	6.92±0.62		0.77±0.09
^{133}I	16.58±2.06	8.50±0.63	4.26±0.53	1.20±0.17
^{135}I (^{135}Xe)	17.44±2.14	9.86±0.58	6.89±0.67	1.22±0.16
^{136}Cs				
^{139}Ba	16.46±1.56	10.22±0.44	6.75±0.30	1.71±0.19
^{140}Ba (^{140}La)		7.54±0.56	5.00±0.46	1.03±0.18
^{141}Ce	15.33±2.46			
^{142}La	13.05±1.12	5.83±0.39	4.38±0.36	0.70±0.24
^{143}Ce	12.86±1.10	6.24±0.36		0.84±0.07
^{149}Nd	5.21±0.84	2.45±0.40	2.85±0.47	0.39±0.08
^{151}Pm				
^{153}Sm			1.13±0.31	

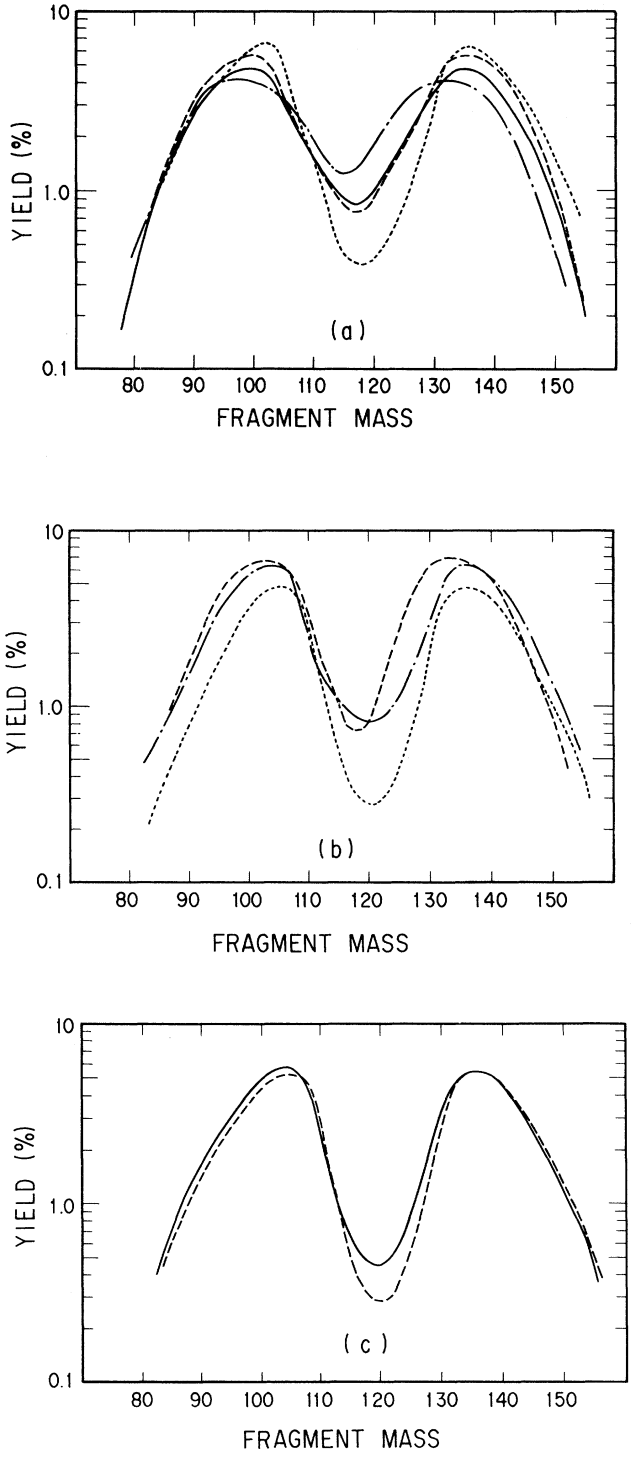

FIG. 5(a) Mass yield curve for the compound nucleus $Z=93$ at the excitation energy around 16 MeV. Dot-dashed line for $^{233}U+p$, solid line for $^{235}U+p$, dashed line for $^{236}U+p$, and dotted line for $^{238}U+p$ (taken from Ref. [18]). (b) Mass yield curve for the compound nucleus $Z=95$ at the excitation energy around 16 MeV. Dashed line for $^{239}Pu+p$, dot-dashed line for $^{242}Pu+p$, and dotted line for $^{244}Pu+p$. (c) Mass yield curve for the compound nucleus $Z=96$ at the excitation energy around 16 MeV. Solid line for $^{241}Am+p$, dashed line for $^{243}Am+p$.

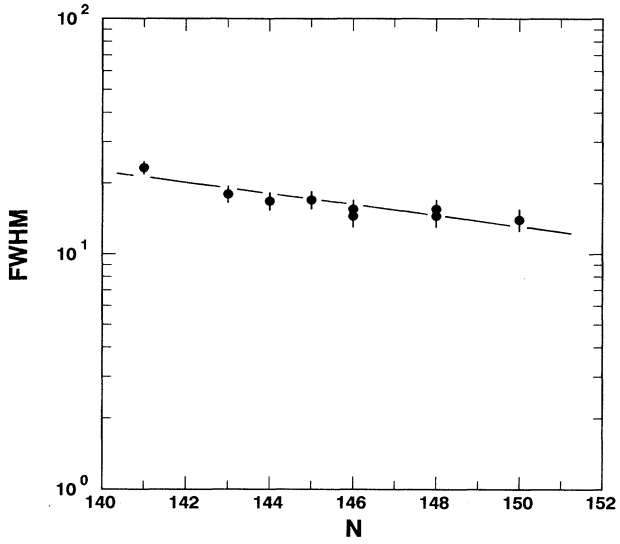

FIG. 6. Full width at half maximum (FWHM) of the heavy asymmetric peak for the excitation energy of around 16 MeV as a function of neutron number of the compound nucleus.

peak, and the peak-to-valley ratio. For systematic comprehension, mass yield curves of the $^{232}Th+p$ (Ref. [17]) and the $^{238}U+p$ (Ref. [18]) are also included in the discussion.

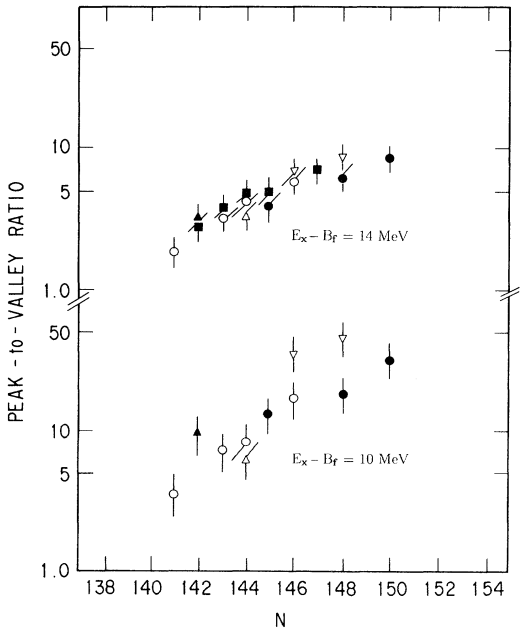

FIG. 7. Variation of the peak-to-valley ratio as a function of neutron number of the compound nucleus with the same excitation energy of 10 and 14 MeV above the fission barrier: ○ for $Z=93$, ▲ for $Z=91$, △ for $Z=94$, ● for $Z=93$, ■ for $Z=92$ (taken from Ref. [6]), and ▽ for $Z=96$.

A. Weighted mean mass of asymmetric peak

Weighted mean mass numbers of the asymmetric peaks for the excitation energy of the compound nucleus of 16 MeV were evaluated by following relationship:

$$\overline{A} = \sum(A_i Y_i)/\sum Y_i \ , \tag{2}$$

where A_i is the appropriate mass number and Y_i is the corresponding fission yield. The mean masses are shown in Fig. 3. As the mean mass of the actual fissioning nuclide could not be determined experimentally in the present study, the mass of the compound nucleus is shown as A_f. They are different by no more than two mass units in the proton energy range of the present work. The weighted mean mass numbers reported in literature are also shown in the same figure for thermal-neutron-induced fissions and spontaneous fissions. It has been known for thermal-neutron-induced fissions and spontaneous fissions that the peak position of the heavier asymmetric peak always stays at $A = 134-142$ due to the strong shell of $N = 82$ or $Z = 50$ or both. The present results are in agreement with this trend, although the

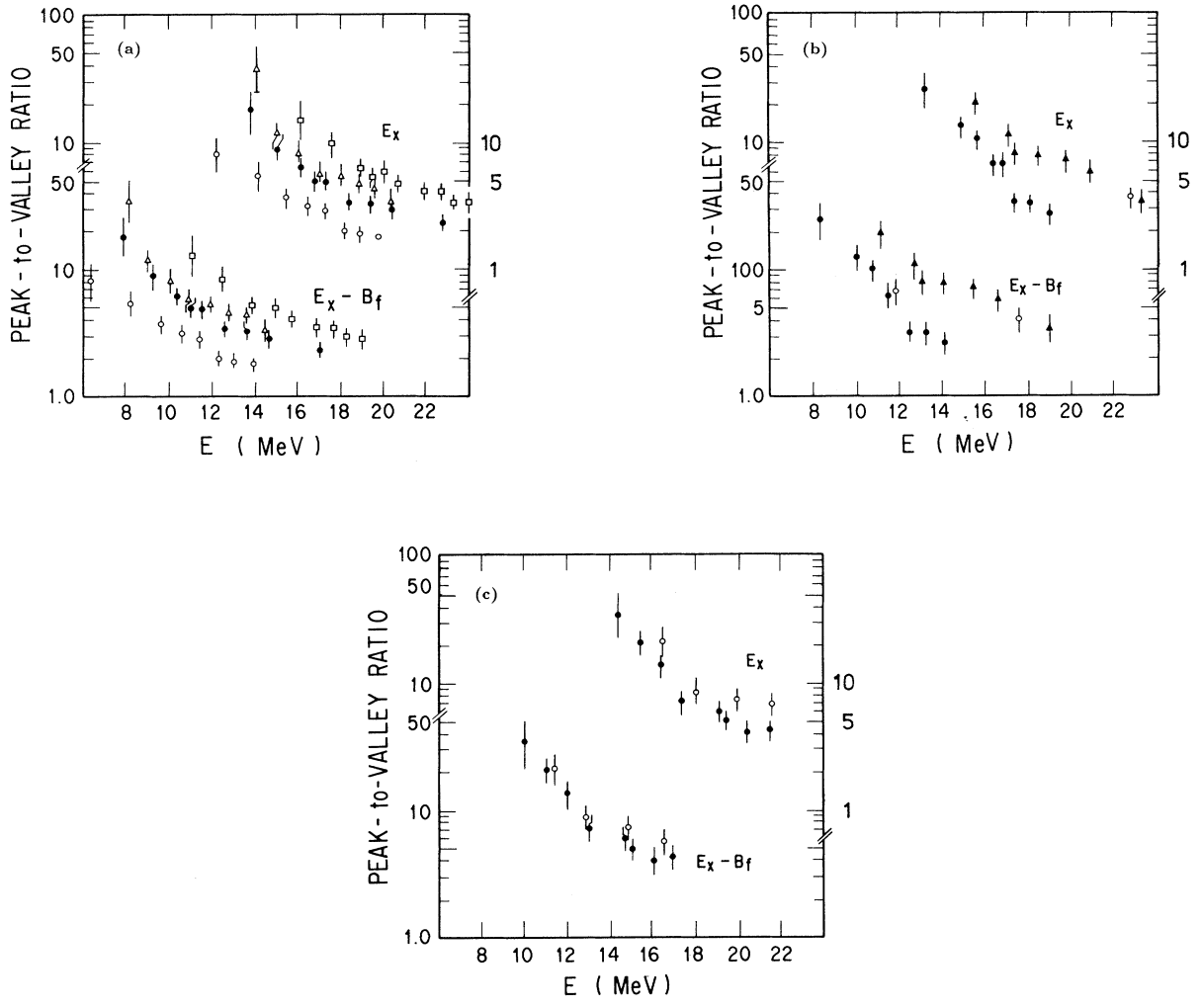

FIG. 8. (a) Variation of the peak-to-valley ratio for compound nucleus of the same $Z = 93$ as a function of the excitation energy; ○ for $^{233}U+p$, ● for $^{235}U+p$, △ for $^{236}U+p$, and □ for $^{238}U+p$ (Ref. [18]). Upper part shows the peak-to-valley ratios as a function of the compound nucleus and lower part indicates those as a function of the excitation energy above the fission barrier. (b) Variation of the peak-to-valley ratio for compound nucleus of the same $Z = 95$ as a function of the excitation energy; ● for $^{239}Pu+p$, ○ for $^{242}Pu+p$, and ▲ for $^{244}Pu+p$. Upper part shows the peak-to-valley ratios as a function of the compound nucleus and lower part indicates those as a function of the excitation energy above the fission barrier. (c) Variation of the peak-to-valley ratio for compound nucleus of the same $Z = 96$ as a function of the excitation energy; ● for $^{241}U+p$ and ○ for $^{243}U+p$. Upper part shows the peak-to-valley ratios as a function of the compound nucleus and lower part indicates those as a function of the excitation energy above the fission barrier.

weighted mean mass for proton-induced fission is somewhat smaller especially for smaller A_f. The latter may be related with the smaller peak-to-valley ratio in proton-induced fission, especially at higher excitation energy. In order to see the isotopic trend of the weighted mean mass number, the present results are also plotted as a function of A_f and neutron number (N) in Fig. 4. From the figure, both of the light and heavy weighted mean mass number are found to become larger with increased A_f and N. Their Z dependence is also noticeable.

B. FWHM of asymmetric peak

Mass yield curves obtained by drawing a line through the data points by eye are shown for comparison among the fissioning nuclei of the same Z in Figs. 5(a)–5(c) for the excitation energy of the compound nucleus of around 16 MeV. Mass yield curves change systematically as a function of neutron number. The depth of the valley region (symmetric region) decreases and the width of the asymmetric peak becomes narrower with an increase of the neutron number of the fissioning nucleus for all Z. The full widths at the half maximum (FWHM) of the heavier asymmetric peaks observed for the excitation energy of 16 MeV are shown in Fig. 6 as a function of neutron number. The errors of 5–7 % were estimated from the ambiguity in determining the peak top value. It is found that the FWHM values decrease exponentially with an increase of neutron number. This fact shows that the FWHM of a mass yield curve is strongly influenced by the neutron number of the fissioning nucleus, and not much by the Z value.

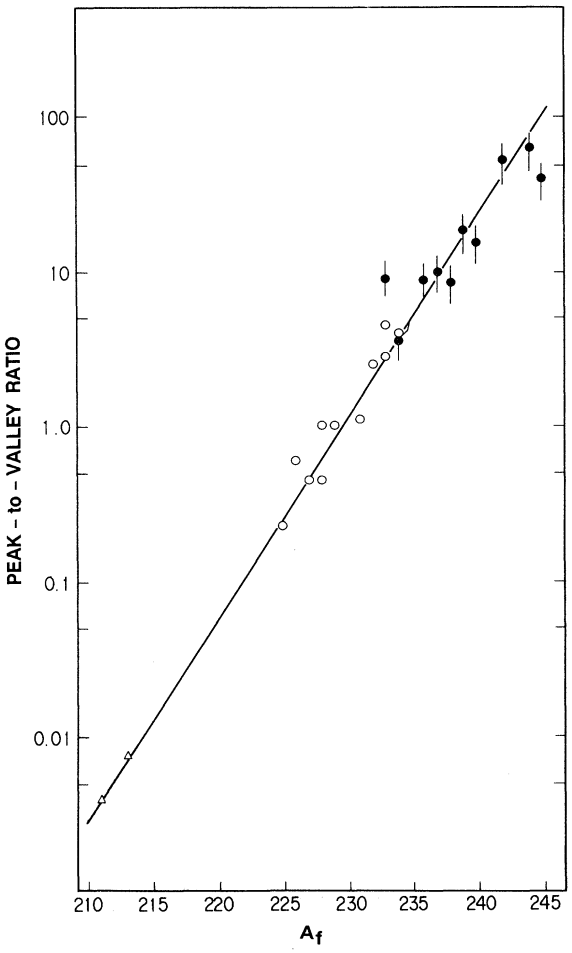

FIG. 9. Peak-to-valley ratio for the same excitation energy of 9.5 MeV above the fission barrier as a function of the fissioning nuclide. Solid circles are for the values obtained in this work, open circles and open triangles for the asymmetric-to-symmetric yield ratios by Specht (Ref. [26]) and by Itkis *et al.* (Ref. [27]), respectively.

C. Peak-to-valley ratio

The so-called peak-to-valley ratio is a frequently used index for measuring the degree of the asymmetric (or symmetric) nature of mass division [2,19–24]. It is the ratio of the peak yield of the mass distribution to the lowest yield at the symmetry valley. The peak-to-valley ratios observed for the excitation energies of 10 and 14 MeV above the fission barrier are plotted in Fig. 7 as a function of the neutron number of a compound nucleus. The values were obtained from the smooth curve drawn through the experimental and the reflected data points. The error attached to each point was estimated from the errors in drawing the smoothed curve at the peak and the valley region. For fission barrier heights (B_f), the values presented by Back *et al.* [25] were used. It is clearly shown that the peak-to-valley ratio systematically increases as the neutron number of the fissioning nucleus increases. This trend is in agreement with that reported for the 14.8 MeV neutron-induced fission of uranium isotopes by Nethaway and Mendoza [6]. It is also to be pointed out that the peak-to-valley ratios for ^{233}Pa, ^{242}Cm, and ^{244}Cm at $E_x - B_f = 10$ MeV are larger than those for Np and Am isotopes even though the neutron number of the compound nucleus is the same. This fact indicates that they are dependent also on the Z of the fissioning nucleus. Variation of the peak-to-valley ratio as a function of the excitation energy of the compound nucleus and the excitation energy above the fission barrier are shown in Figs. 8(a), 8(b), and 8(c) for the isotopes of neptunium, americium, and curium, respectively. The peak-to-valley ratios decrease and tend to level off as the excitation energy is increased for all isotopes. Finally, the peak-to-valley ratios observed for fixed excitation energies above fission barriers are plotted in logarithmic scale in Fig. 9 for a wider range of A_f by using literature values. Filled circles show the peak-to-valley ratios observed in the present work for the excitation energy of 9.5 MeV above the fission barrier. Open circles are those taken from the experimental data by Specht [26] for the excitation energy of 9.5 MeV above the fission barrier. They are not peak-to-valley ratios but the yield ratios of the asymmetric to symmetric fission calculated from the peak areas of the triple humped-mass yield curves. Open triangles are the ratios of the asymmetric to symmetric reported by Itkis *et al.* [27]. Strictly speaking, the peak-

to-valley ratios of the present study and the yield ratios of the asymmetric-to-symmetric reported by other workers may not have the same physical meanings. The two ratios may have the same physical meaning if two independent fission modes of asymmetric and symmetric fission are assumed, and if the shape of the mass yield curve of each mode is not strongly dependent on the excitation energy. But it is curious to note that all the data points for the 9.5-MeV excitation energy above the fission barrier fall on a straight line, roughly speaking, as shown in the figure by a solid line. This may indicate that the gross feature of mass division changes exponentially as a function of A_f from the fission of $Z=84$ up to $Z=96$.

V. CONCLUSION

Mass yield curves in low-energy proton-induced fission of ^{233}U, ^{235}U, ^{236}U, ^{237}Np, ^{239}Pu, ^{242}Pu, ^{244}Pu, ^{241}Am, and ^{243}Am were measured for several incident energies. Some characteristics of the mass yield curves have been compared either at the same excitation energy or for the same Z with different N of the compound nucleus. The results can be summarized as follows: (1) The weighted mean mass numbers of the lighter and heavier asymmetric peaks are almost in agreement with those for thermal-neutron-induced fission and spontaneous fission of the same A_f. (2) The FWHM of the heavier asymmetric mass yield peak varies as a function of the neutron number of the fissioning nucleus. (3) The peak-to-valley ratios are strongly dependent on the excitation energy as expected. Those for the same excitation energy above the fission barrier are clearly dependent on the neutron number of the fissioning nucleus and slightly also on the atomic number. If the peak-to-valley ratios are considered synonymous with the ratios of the asymmetric-to-symmetric fission yields, they are found to change, as a first approximation, exponentially from the fission of $Z=84$ up to that of $Z=96$.

ACKNOWLEDGMENTS

The authors wish to thank the staff and crew of the Japan Atomic Energy Research Institute (JAERI) Tandem Accelerator and the AVF Cyclotron of Institute for Nuclear Study (INS). We would like to thank H. Matsuoka, S. Motoishi, S. I. Ichikawa, Dr. H. Kudo, and Dr. H. Umezawa of the Department of Radioisotopes of JAERI for helpful advice and support.

*Present address: Laboratory of Nuclear Science, Faculty of Science, Tohoku University, 1-2-1 Mikamine, Taihaku-ku, Sendai, Miyagi, 982 Japan.

[1] E. K. Hyde, *Nuclear Properties of Nuclear Fission* (Prentice-Hall, Englewood Cliffs, NJ, 1964), Vol. III.
[2] H. R. Von Gunten, Actinides Rev. **1**, 275 (1969).
[3] J. P. Unik, J. E. Gindler, L. E. Glendenin, K. F. Flynn, A. Gorsky, and R. K. Sjoblom, *Physics and Chemistry of Fission 1973* (IAEA, Vienna, 1974), Vol. II, p. 19.
[4] H. Nakahara and T. Ohtsuki, J. Radioanal. Nucl. Chem. **142**, 231 (1990).
[5] D. C. Hoffman, Nucl. Phys. **A502**, 21c (1989).
[6] D. R. Nethaway and B. Mendoza, Phys. Rev. **6**, 1821 (1972).
[7] C. Wagemans, P. Schllerbeeckx, and A. Deruytter, Nucl. Phys. **A502**, 287c (1989).
[8] R. Collé, R. Kishore, and J. B. Cumming, Phys. Rev. C **9**, 1819 (1974).
[9] C. F. Williamson, J. P. Bougot, and J. Picard, Centre d'Etudes Nucleaires de Saclay Report No. CEA-R3042, 1966 (unpublished).
[10] L. C. Northcliffe and R. F. Schilling, Nucl. Data Sect. A **7**, 233 (1970).
[11] F. Plasil and M. Blann, Phys. Rev. C **11**, 508 (1975).
[12] J. H. McHugh and M. C. Michel, Phys. Rev. **172**, 1160 (1968).
[13] G. L. Bate and J. R. Huizenga, Phys. Rev. **133**, B1471 (1964).
[14] V. N. Kononov, E. D. Poletaev, and P. P. D'yachenko, Yad. Fiz. **27**, 298 (1978) [Sov. J. Nucl. Phys. **27** 162 (1978)].
[15] G. R. Choppin, J. R. Meriwether, and J. D. Fox, Phys. Rev. **131**, 2149 (1963).
[16] P. Polak and A. H. W. Aten, Jr., J. Inorg. Nucl. Chem. **42**, 641 (1979).
[17] H. Kudo, H. Muramatsu, H. Nakahara, K. Miyano, and I. Kohno, Phys. Rev. C **25**, 3011 (1982).
[18] Y. Hamajima *et al.* (unpublished).
[19] T. Ohtsuki, Y. Hamajima, K. Sueki, H. Nakahara, Y. Nagame, N. Shinohara, and H. Ikezoe, Phys. Rev. C **40**, 2144 (1989).
[20] L. E. Glendenin, J. E. Gindler, I. Ahmad, D. J. Henderson, and J. W. Meadows, Phys. Rev. C **22**, 152 (1980).
[21] R. Eaker, H. S. Plendl, A. F. Zeller, A. Clem, L. Muga, and J. M. Nicovich, Phys. Rev. C **20**, 1055 (1979).
[22] C. F. Tsang and J. B. Wilhelmy, Nucl. Phys. **A184**, 417 (1972).
[23] H. Baba and S. Baba, Nucl. Phys. **A175**, 199 (1971).
[24] H. A. Tewes and R. A. James, Phys. Rev. **88**, 860 (1952).
[25] B. B. Back, Ole Hansen, H. C. Britt, J. D. Garrett, and B. Leroux, *Physics and Chemistry of Fission 1973* (IAEA, Vienna, 1974), Vol. I, p. 3.
[26] H. J. Specht, Nucleonika, **20**, 717 (1975).
[27] M. G. Itkis, V. N. Okolovich, A. Ya. Rusanov, and G. N. Smirenkin, Yad. Fiz. **47**, 1201 (1988) [Sov. J. Nucl. Phys. **47**, 765 (1988)].